Saddle points and dynamics of Lennard-Jones clusters, solids, and supercooled liquids

Jonathan P. K. Doye[a)] and David J. Wales[b)]
University Chemical Laboratory, Lensfield Road, Cambridge CB2 1EW, United Kingdom

The properties of higher-index saddle points have been invoked in recent theories of the dynamics of supercooled liquids. Here we examine in detail a mapping of configurations to saddle points using minimization of $|\nabla E|^2$, which has been used in previous work to support these theories. The examples we consider are a two-dimensional model energy surface and binary Lennard-Jones liquids and solids. A shortcoming of the mapping is its failure to divide the potential energy surface into basins of attraction surrounding saddle points, because there are many minima of $|\nabla E|^2$ that do not correspond to stationary points of the potential energy. In fact, most liquid configurations are mapped to such points for the system we consider. We therefore develop an alternative route to investigate higher-index saddle points and obtain near complete distributions of saddles for small Lennard-Jones clusters. The distribution of the number of stationary points as a function of the index is found to be Gaussian, and the average energy increases linearly with saddle point index in agreement with previous results for bulk systems. © *2002 American Institute of Physics.*
[DOI: 10.1063/1.1436470]

I. INTRODUCTION

The properties of the potential energy surface (PES), or landscape, of supercooled liquids and glasses have been the focus of much recent theoretical research into glasses. The origins of this approach date back to Goldstein, who suggested that the dynamics could be separated into vibrational motion about a minimum on the PES and transitions between minima.[1] This idea led to the pioneering ''inherent structure'' approach of Stillinger and co-workers.[2,3] In this approach the PES is partitioned into basins of attraction surrounding the minima (inherent structures), where a basin of attraction is defined as the set of points for which steepest-descent pathways lead to the same minimum. This mapping allows a conceptual framework to be built in which the role of the minima can be separated from the effects of vibrational motion. The dynamics can then be viewed in terms of the transitions between these basins which occur when the system passes along a transition state valley. Therefore, from the inherent structure point of view the key points on the PES are the minima and transition states, which are defined as stationary points with Hessian index one, i.e., one negative eigenvalue. Higher-index saddle points (with $I \geqslant 2$ negative eigenvalues) need not be considered in this description, because, by the Murrell–Laidler theorem, if two minima are connected by an index two saddle, then there must be a lower-energy path between them involving only true transition states.[4]

This inherent structure approach has provided important insights into the behavior of supercooled liquids and glasses,[5,6] as well as clusters,[7] and biomolecules.[8] For example, changes in the dynamics of supercooled liquids as the temperature is decreased must correspond to descent down

the PES to lower-energy minima.[9] Furthermore, a careful investigation of the density dependence of the properties of the sampled minima has suggested how changes in the PES can lead to a change in the dynamics from strong to fragile.[10] This approach has also been applied to investigate nonequilibrium properties: Aging involves a slow decrease in the energy of the sampled minima as the system heads towards equilibrium.[11,12]

Much of the above work has focused on the potential energy landscape as sampled under particular conditions of density and temperature. It is also of interest to determine the fundamental characteristics of the landscape, which is, of course, independent of temperature, atomic masses, and coordinate system. For example, one of the most important properties is the distribution of minima. Exhaustive enumeration of the minima of small systems[13,14] seems to confirm the theoretical conjecture that the number of minima increases exponentially with size.[2,15] The distribution of minima as a function of the potential energy can also be obtained by inverting simulation data. This inversion was first performed for a medium-sized cluster,[16] and later for model glasses[17,18] revealing that the distribution is Gaussian. This technique has since been applied to supercooled water[19] and silica.[20] More recently, attention has begun to focus on the harder task of characterizing the distributions of transition states and the resulting barriers.[21,22]

Alternatives to the inherent structure approach have been proposed. In the instantaneous normal mode theory, developed by Keyes and co-workers,[23] the focus is on the spectrum of Hessian eigenvalues for instantaneous configurations. It is argued that diffusion and the associated barriers are related to the negative eigenvalues of this spectrum, although this idea has been the subject of some debate.[24–26] Many of the negative eigenvalues result from the anharmonicity within a well, however, once these are removed, simu-

[a)]Electronic mail: jon@clust.ch.cam.ac.uk
[b)]Electronic mail: dw34@cam.ac.uk

lations have indicated that the number of diffusive directions in a supercooled liquid tends towards zero near to the mode-coupling temperature.[27,28]

Another recent proposal emphasizes the role of higher-index stationary points on the PES, and attempts to explain the origins of strong and fragile liquids in these terms.[29] One of the underlying ideas is that as the size of the system becomes large, most of the configuration space volume in a basin of attraction is concentrated near to the borders of that basin, and so a randomly chosen point is more likely to lie closer to a saddle point than to a minimum.[30] Therefore, the proposal is to divide the potential energy surface into "basins of attraction" that surround stationary points of any index. However, with the steepest-descent mapping of the inherent structure approach, the basins of attraction only surround minima, and convergence to a higher-index saddle point can only occur when the starting point lies exactly on the boundary between two basins of attraction. The volume associated with these boundaries is of measure zero. Therefore, a different mapping is required to divide configuration space in the desired way. Borrowing a trick that has been previously used to locate transition states,[31,32] a mapping has been suggested in which steepest-descent paths on the function $|\nabla E|^2$, the modulus of the gradient of the energy squared, are followed.[33,34] Stationary points on the PES of any index correspond to minima of this new function.

From the above mapping it was found that below the mode-coupling[35–37] temperature, T_c, the system samples minima but that above this temperature the average saddle point index increases linearly with temperature.[33,34] Such behavior has been interpreted as a transition from dynamics between basins of minima to dynamics between basins of saddles. This approach is becoming more widely applied.[38–42] For example, it has been used to analyze the dynamics of aging. After a quench or crunch (a sudden increase in density) to a state that lies below T_c for that density, initially the system is associated with saddle points whose index decreases logarithmically with time until a crossover time is reached when the system resides near to minima.[39,40]

Here we look in more detail at the $|\nabla E|^2$ mapping and how well it achieves its aim of dividing configuration space into neighborhoods around stationary points of any index. We first examine in Sec. II a model two-dimensional energy surface that can easily be visualized. Then, in Sec. III we study the properties of the mapping for a much-studied binary Lennard-Jones (LJ) system. Given the problems with the $|\nabla E|^2$ mapping we then follow an alternative approach to studying the properties of higher-index saddle points. In Sec. IV we obtain near complete distributions of saddle points for small Lennard-Jones clusters and then analyze their properties. Finally, we conclude with a discussion of some of the issues raised by our results in relation to recent work.

II. MÜLLER–BROWN SURFACE

We first examine the effect of the $|\nabla E|^2$ mapping for a model two-dimensional energy surface that we can easily visualize. We use the Müller–Brown surface,[43] which has the form
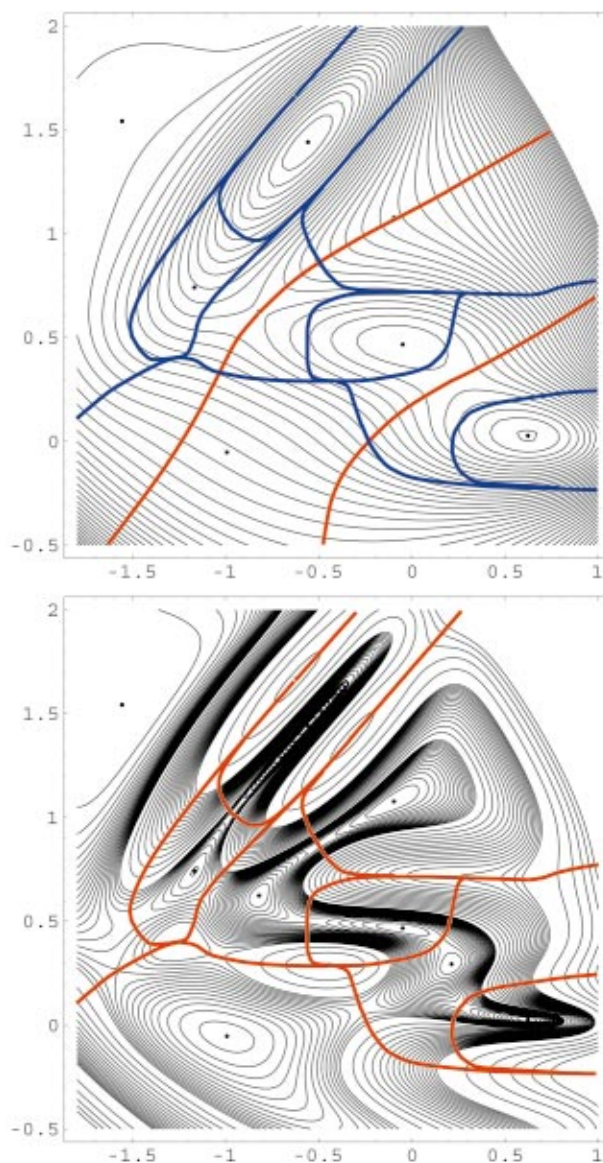

FIG. 1. (Color) Contour diagrams of (a) E and (b) $|\nabla E|^2$ for the Müller–Brown surface. The red lines divide the surfaces into basins of attraction surrounding each minimum. In (a) the basin boundaries of $|\nabla E|^2$ have been superimposed in blue. Points have been added corresponding to in (a) the minima of $|\nabla E|^2$ and in (b) the maxima and minima of $|\nabla E|^2$. In (b) contours occur every 1000 in the range 0–20 000, then every 5000 up to 100 000 and finally every 50 000 beyond that range.

$$E(x,y)=\sum_{i=1}^{4} A_i \exp[a_i(x-x_i^0)^2+b_i(x-x_i^0)(y-y_i^0)$$
$$+c_i(y-y_i^0)^2], \qquad (1)$$

where

$$A=(-200,-100,-170,15), \quad a=(-1,-1,-6.5,0.7),$$
$$b=(0,0,11,0.6), \quad c=(-10,-10,-6.5,0.7), \qquad (2)$$
$$x^0=(1,0,-0.5,-1), \quad y^0=(0,0.5,1.5,1).$$

This surface has been used as a test system for local optimization algorithms and its properties have been thoroughly examined.[44–48]

TABLE I. Minima of $|\nabla E|^2$ for the Müller–Brown surface. Those that are also stationary points of E are labeled SP, and those that are not are labeled NSP. The index, I, is the number of negative eigenvalues of the Hessian at that point.

	I	E	$|\nabla E|^2$	x	y
SP1	0	−146.700	0.0	−0.558	1.442
SP2	0	−108.167	0.0	0.623	0.028
SP3	0	−80.768	0.0	−0.050	0.467
SP4	1	−72.249	0.0	0.212	0.293
SP5	1	−40.665	0.0	−0.822	0.624
NSP1	0	−56.235	10 892.8	−1.169	0.741
NSP2	0	19.057	175.2	−1.559	1.543
NSP3	1	21.394	5018.2	−0.097	1.076
NSP4	0	27.070	6533.2	−0.995	−0.053

Contour plots of E and $|\nabla E|^2$ are shown in Fig. 1 and information concerning the minima of $|\nabla E|^2$ are given in Table I.[49] The section of the energy surface that we consider has five stationary points: three minima and the two transition states that connect them. Stationary points of the $|\nabla E|^2$ surface satisfy $2\mathbf{Hg}=\mathbf{0}$, where $\mathbf{H}$ is the Hessian (second derivative matrix) and $\mathbf{g}=\nabla E$ is the gradient vector. Obviously, stationary points of the PES have $|\nabla E|^2=0$, and so correspond to minima of $|\nabla E|^2$. However, there are additional minima on the $|\nabla E|^2$ surface with $|\nabla E|^2>0$, where $\mathbf{g}$ is an eigenvector of $\mathbf{H}$ with zero eigenvalue, i.e., there is an inflection point in the direction of the gradient. We will refer to these two types of $|\nabla E|^2$ minima by the labels SP (stationary point of E) and NSP (nonstationary point of E). There are four such NSP's on the Müller–Brown surface. The possibility of NSP's has been previously noted in Refs. 29, 33, and 34, however, it was claimed that their effect was negligible.[33]

A further property of the NSP's is that they must lie on a gradient extremal, one definition of which is $\mathbf{Hg}=\lambda\mathbf{g}$. Gradient extremals are curves for which each point is an extremum of $|\nabla E|\equiv|\mathbf{g}|$ along the corresponding energy contour. The gradient extremals for the Müller–Brown surface have been calculated in Ref. 47.

The basins of attraction associated with the SP's and NSP's on the $|\nabla E|^2$ surface are shown in Fig. 1. For the region of configuration space that we depict here, the majority of this space corresponds to basins of attraction associated with NSP's. Although much of this configuration space has a relatively high energy, the NSP basins of attraction do extend into some low-energy regions. In particular, NSP1 is lower in energy than the transition state SP5, and on moving away from the minimum SP1 along the softest mode, the first new basin of attraction that is encountered corresponds to NSP1. Furthermore, the basins of attraction associated with NSP2 and NSP3 extend below the energy of SP5 into regions corresponding to the walls of the basin of attraction associated with SP1 on the original surface. Minimization of $|\nabla E|^2$ for points from these regions will lead to a considerable increase in energy.

It is clear from Fig. 1 that the $|\nabla E|^2$ surface is much more rugged than the original energy surface. First, the surface has more minima. Second, the ratio of maximum to minimum nonzero Hessian eigenvalues of the $|\nabla E|^2$ function at SP's has a magnitude that is roughly the square of the corresponding ratio for stationary points of E, because the second derivative of $|\nabla E|^2$ includes a product of the original Hessian matrix. For SP1 this ratio is ∼100 and so the well surrounding SP1 on the $|\nabla E|^2$ surface is extremely asymmetric and narrow.

This second feature of the $|\nabla E|^2$ surface has important practical consequences. In the language of optimization theory, such points are said to be ill-conditioned,[50] and so even simple minimization of $|\nabla E|^2$ is likely to be rather slow. These effects will be further examined when we consider a binary LJ system in Sec. III.

Although the Müller–Brown surface is not a physical example, it does suggest that the division of configuration space into basins of attraction surrounding the minima of $|\nabla E|^2$ could be problematic.

III. BULK BINARY LENNARD-JONES

Binary Lennard-Jones (BLJ) mixtures have been extensively studied in an effort to elucidate the complex phenomenology of glasses, as they do not crystallize on the molecular dynamics (MD) time scale when suitably parameterized.[9–12,17,18,21,22,27,33,34,51–61] Most of these investigations have reported changes in behavior around the critical temperature predicted by mode-coupling theory,[35–37] which is calculated as $T_c\approx0.435$ for the mixture we consider here.[52,56] For example, Sastry, Debenedetti, and Stillinger[9] presented evidence that nonexponential relaxation starts below about $T=1$, while the height of the effective barriers to relaxation increases significantly around $T=0.45$. They view the regions below $T=1$ and $T=0.45$ as "landscape-influenced" and "landscape-dominated" regimes, respectively. They also found that local minima obtained by quenching from configurations generated at $T=0.5$ could escape to different local minima much more easily than local minima obtained from configurations generated at $T=0.4$.

Using an instantaneous normal modes picture Donati, Sciortino, and Tartaglia also concluded that activated dynamics becomes important around T_c.[27] Schrøder et al. found that the liquid dynamics could be separated into transitions between minima and vibrational motion[1] at a similar temperature,[51] and correlated motions of atoms in groups that grew with decreasing temperature were reported by some of the same workers.[58] Two different groups have recently reported that the typical Hessian index of stationary points sampled by BLJ systems extrapolates to zero, again

TABLE II. Mean total energy, E, potential energy, PE, kinetic energy, KE, and kinetic equipartition temperature, T, for the MD runs. The $\pm$ values represent one standard deviation. #min, #ts and #G2 are the number of distinct minima, transition states and stationary point of $|\nabla E|^2$ found for 10^3 searches (excluding permutational isomers), as described in the text. %SP and %NSP are the percentage of quenches on the $|\nabla E|^2$ surface that converged to stationary points and nonstationary points of E, respectively (out of 10^3 total).

Run	E	PE	KE	T	#min	#ts	#G2	%SP	%NSP
				256-atom supercell					
1	-1699.879 ± 0.002	-1753 ± 2	53 ± 2	0.138 ± 0.005	54	274	740	1.6	98.4
2	-1599.268 ± 0.005	-1704 ± 4	105 ± 4	0.276 ± 0.010	46	509	909	9.6	90.4
3	-1500.070 ± 0.008	-1656 ± 6	156 ± 6	0.409 ± 0.015	280	789	1000	1.8	98.2
4	-1399.487 ± 0.011	-1594 ± 7	194 ± 7	0.510 ± 0.019	987	1000	1000	3.2	96.8
5	-1301.872 ± 0.015	-1540 ± 9	238 ± 9	0.625 ± 0.023	984	1000	1000	3.0	97.0
6	-1201.004 ± 0.020	-1485 ± 11	284 ± 11	0.745 ± 0.028	991	1000	1000	4.8	95.2
7	-1098.883 ± 0.025	-1431 ± 12	332 ± 12	0.871 ± 0.032	995	1000	1000	5.9	94.1
8	-999.982 ± 0.031	-1380 ± 14	380 ± 14	0.997 ± 0.036	994	1000	1000	4.8	95.2
				320-atom crystal					
1	-2192.679 ± 0.002	-2270 ± 2	78 ± 2	0.162 ± 0.002	1	39	1	100.0	0.0
2	-1992.690 ± 0.007	-2175 ± 6	182 ± 6	0.382 ± 0.012	1	49	2	99.4	0.6
3	-1792.710 ± 0.013	-2082 ± 9	289 ± 9	0.606 ± 0.019	1	56	10	91.0	9.0
4	-1592.739 ± 0.020	-1989 ± 12	397 ± 12	0.831 ± 0.026	1	64	55	66.4	33.6
5	-1392.773 ± 0.034	-1889 ± 16	496 ± 16	1.041 ± 0.034	187	721	860	25.5	74.5

around T_c,[33,34] and we will present a more detailed investigation of this behavior below. Our results show that transition states are still accessible below T_c, but support the general consensus that the PES sampled by the BLJ system changes in character somewhere around T_c.

The BLJ mixture that we consider involves a 256-atom supercell containing 205 (80%) A atoms, and 51 (20%) B atoms, with parameters $\sigma_{AA}=1.0$, $\sigma_{AB}=0.8$, $\sigma_{BB}=0.88$, $\epsilon_{AA}=1.00$, $\epsilon_{AB}=1.5$, and $\epsilon_{BB}=0.5$.[52] The units of distance and energy were taken as σ_{AA} and ϵ_{AA}. The chosen box length gives a fixed number density of $1.2\sigma_{AA}^{-3}$, and a cutoff of $2.5\sigma_{AA}$ was used along with the minimum image convention and a shifting/truncation scheme that ensures continuity of the energy and its first derivative, as in previous work.[9,62]

Standard microcanonical molecular-dynamics (MD) simulations of 10^5 equilibration steps, followed by 10^6 data collection steps, were first run using the Verlet propagator at a series of increasing total energies (Table II). The starting point for the first run was the lowest-energy minimum found in previous work,[21] and subsequent runs used the final configuration of the previous trajectory as the starting point. A time step of 0.003 reduced units was employed in each case. Every 1000th configuration from the data collection phase was saved and used as a starting point for the following geometry optimizations: (1) minimization using a modified version of Nocedal's LBFGS algorithm,[63] (2) a transition state search using hybrid eigenvector-following,[7,64,65] (3) minimization of $|\nabla E|^2$ using Nocedal's LBFGS algorithm.[63] The first two searches on the conventional PES employ standard techniques[7] and were followed by between one to three full eigenvector-following steps to converge the root-mean-square (rms) force below 10^{-7} reduced units and check the Hessian index of the stationary point, defined as the number of negative Hessian eigenvalues. All the searches in (1) and (2) are tightly converged to stationary points of the required index with the above tolerance, which is more stringent than the criteria used in Ref. 42.

As pointed out in Sec. II the ratio of the maximum to the minimum eigenvalue of $|\nabla E|^2$ near to an SP makes minimi-

zation of $|\nabla E|^2$ laborious. There is a further problem because the second derivatives of the shifted-truncated BLJ potential[62] are discontinuous at the cutoff, and hence the derivatives of $|\nabla E|^2$ have corresponding discontinuities. Nevertheless, it is possible to converge the $|\nabla E|^2$ minimizations to a root-mean-square force below 10^{-5}, at which point the value of $|\nabla E|^2$ is generally converged to at least nine decimal places. Such accuracy should be acceptable for the present purposes, and was achieved by fixing the neighbor list during minimization for SP's and NSP's close to convergence but suffering from discontinuities. Typically, these minimizations of $|\nabla E|^2$ involve two orders of magnitude more steps than minimizations on the original PES.

In most of the previous work reporting results of $|\nabla E|^2$ minimizations[33,34] details of the calculations, such as the algorithms employed, the convergence criteria or the number of saddles actually found, were not reported. We are, therefore, unable to provide detailed comparisons.

The glass transition temperature for this system under our simulation conditions lies between 0.4 and 0.5, as is evident from the caloric curve (not illustrated) and jumps in various quantities tabulated in Tables II and III. Of course, the precise temperature at which the glass transition occurs depends upon the rate at which the temperature is changed. The number of different minima and transition states located from the 10^3 different starting points decreases markedly on glass formation. However, a significant number of distinct minima and transition states are sampled below the glass transition, as expected from previous work that revealed large numbers of low barrier "nondiffusive" pathways for this system.[21] The fraction of negative eigenvalues, $i=I/(3N-3)$, (the three zero eigenvalues corresponding to translations are excluded) located by minimizing $|\nabla E|^2$ jumps by a factor of about two on melting, and continues to rise approximately linearly at higher temperature. This result is in line with previous calculations for supercooled liquids,[33,34,41] and also with studies based upon instantaneous normal mode analysis.[27] However, in contrast to the findings

TABLE III. Mean energy differences, Δ, and displacements, D, between the starting point and the converged geometry after searching for minima (min), transition states (ts), and minimizing $|\nabla E|^2$ (G2). i_{SP} and i_{NSP} are the fractions of negative Hessian eigenvalues after minimizing $|\nabla E|^2$, split into stationary points and nonstationary points of E, respectively. The $\pm$ values represent one standard deviation.

Run	ΔE_{min}	D_{min}	ΔE_{ts}	D_{ts}	ΔE_{G2}	D_{G2}	$i_{NSP} \times 10^3$	$i_{SP} \times 10^3$
				256-atom supercell				
1	216 ± 17	22.0 ± 1.6	208 ± 17	23.1 ± 2.0	199 ± 16	24.2 ± 1.5	5.1 ± 1.7	4.2 ± 2.1
2	261 ± 22	25.2 ± 0.8	253 ± 22	25.4 ± 1.4	245 ± 22	25.6 ± 1.2	5.4 ± 2.0	5.1 ± 1.3
3	303 ± 64	25.4 ± 1.7	299 ± 62	25.7 ± 1.6	286 ± 85	26.1 ± 1.7	6.7 ± 2.4	5.8 ± 1.7
4	370 ± 37	81.3 ± 6.2	365 ± 36	81.3 ± 6.1	330 ± 34	81.3 ± 6.2	15.0 ± 3.9	12.7 ± 5.5
5	425 ± 40	144.5 ± 10.2	421 ± 40	144.5 ± 10.2	366 ± 38	144.5 ± 10.1	21.3 ± 4.4	19.6 ± 5.2
6	485 ± 46	224.7 ± 12.6	480 ± 46	224.7 ± 12.6	403 ± 44	224.7 ± 12.6	28.0 ± 5.1	27.8 ± 6.0
7	544 ± 48	320.3 ± 16.9	539 ± 48	320.3 ± 17.0	439 ± 45	320.3 ± 16.9	34.5 ± 5.5	34.4 ± 7.1
8	602 ± 56	426.5 ± 22.3	598 ± 56	426.5 ± 22.3	475 ± 52	426.5 ± 22.3	41.0 ± 5.6	42.1 ± 5.5
				320-atom crystal				
1	75 ± 2	8.8 ± 0.04	53 ± 8	9.4 ± 1.1	75 ± 2	8.8 ± 0.3	$\cdots$	0.0 ± 0.0
2	170 ± 6	8.8 ± 0.05	144 ± 10	9.7 ± 1.0	170 ± 6	8.8 ± 0.05	0.0 ± 0.0	0.0 ± 0.0
3	263 ± 9	8.9 ± 0.1	240 ± 13	9.9 ± 1.5	263 ± 9	8.9 ± 0.1	0.0 ± 0.2	0.0 ± 0.2
4	356 ± 12	9.0 ± 0.1	334 ± 16	9.8 ± 1.3	352 ± 13	9.0 ± 0.2	0.2 ± 0.5	0.0 ± 0.2
5	443 ± 15	15.4 ± 3.7	432 ± 18	15.7 ± 3.6	425 ± 20	15.7 ± 3.7	1.6 ± 1.5	1.2 ± 1.3

of Refs. 33, 34, and 41, the value of i does not vanish, even for our low-temperature glassy configurations.

Throughout the temperature range studied here the vast majority of minimizations of $|\nabla E|^2$ converge to NSP's. The largest percentage of SP's occurs for run 2, but this is probably a fluctuation caused by the nonergodic nature of the low temperature simulations. Similarly, in Ref. 34 NSP's were said to be "frequently sampled" and these points were excluded from the calculated properties. By contrast, in Ref. 33 the number of NSP's was said to be "negligible with respect to the number of true saddles." However, stimulated by the current results, the authors of this paper have now identified the source of this discrepancy. A reanalysis of their original results has confirmed that the majority of the $|\nabla E|^2$ minima that they found were in fact NSP's.[38]

For each run we find the mean energy differences between the starting point and the structures obtained after searching for minima (min), transition states (ts) and minimizing $|\nabla E|^2$ (G2) are in the order $\Delta E_{min} > \Delta E_{ts} > \Delta E_{G2}$. Hence, in terms of energy, the system is closer to points found by minimizing $|\nabla E|^2$ than it is to minima and transition states, especially at high temperature. This result is unsurprising. By the same logic as the Murrell–Laidler theorem[4] one expects the average potential energy of a stationary point to increase with I.

However, the Euclidean distance between the above points is practically the same for all three searches (we checked that the center-of-mass did not change during geometry optimization). In terms of distance, the system seems to be equally close to a minimum, a true transition state, and an SP or NSP at all temperatures, Therefore, it cannot simply be claimed that the $|\nabla E|^2$ mapping takes the system to its nearest stationary point. These results seem to contrast with the behavior for a spin glass, namely the p-spin spherical model, for which the closest minimum is significantly further away from an equilibrium configuration than is the closest saddle when the system is above the glass transition.[66] For this model the distance to the closest saddle was also reported to be independent of temperature, again seeming to differ from

our results for a structural glass (Table III). However, the mappings that we have employed in our calculations do not necessarily locate the closest stationary point of a given type.

To check that our results do not depend significantly on the minimization algorithm employed we repeated some of the $|\nabla E|^2$ minimizations using a true steepest-descent approach. Both fifth-order Runga–Kutta and Bulirsch–Stoer algorithms were considered,[67] with the former method proving to be the more efficient, although it still required between 10^2 and 10^3 times more steps than LBFGS minimization.[63] To reduce the computational cost we used fifth-order Runga–Kutta integration of the steepest-descent equations for order 10^5 steps and then switched to LBFGS minimization.[63] For 100 regularly spaced starting points from trajectories 1 and 8 the statistics produced by this alternative minimization scheme were very similar to the results in Tables II and III.

We have also generated results for the BLJ crystal with space group $I4/mmm$, which we have recently described elsewhere.[68] Here the supercell consists of 320 atoms with box lengths of 6.1698 (twice) and 7.0053; the other parameters are the same as above, with 256 A and 64 B atoms. Configurations were saved from five MD runs of 10^6 steps each, with 10^5 steps of equilibration, as for the smaller system. The solid is superheated, and only escapes from the crystal in the highest energy run on this time scale (Table II). The fraction of NSP located in $|\nabla E|^2$ minimizations increases systematically from zero at the lowest energy, where each minimization finds the crystal. The I values associated with these runs are all much lower than for the smaller supercell, indicating that the linear rise in I above a threshold temperature that has been observed for supercooled liquids is not simply a universal effect of temperature, but is specific to that region of configuration space. However, stationary points of index up to four are located in run four, where the system still does not escape from a single permutational isomer of the crystal. On minimizing the energy from all the $|\nabla E|^2$ stationary points located in the latter run 97.8% relax to the crystal, but nine other minima are also found. This

result simply reflects the fact that minimizing $|\nabla E|^2$ can raise the energy sufficiently for the configuration to escape from the crystal, even though the system is trapped there on a long time scale.

In view of the above results, and the dominance of NSP's on minimizing $|\nabla E|^2$, we question whether the dynamics of a supercooled liquid can usefully be described in terms of the basins of attraction of $|\nabla E|^2$. Most of these basins do not correspond to stationary points of E at all for the present system. It is also interesting to note that a more recent study instead used a "Newton" method to locate stationary points of any index.[41] This approach can potentially avoid the NSP problem, however few details were provided and the nature of this new mapping should also be carefully examined.

Furthermore, the configuration does not appear to be closer (in terms of distance) to stationary points of any particular index as the temperature varies. Although our results do not support the claim that I vanishes at a well-defined temperature above the glass transition, they do confirm that there is a dramatic decrease in the number of different local minima sampled around this point. Since the prediction that I should vanish below a threshold energy is a mean-field result,[69] it is perhaps not surprising that it is not precisely obeyed. Similarly, the relaxation time scale for structural glasses does not actually diverge at T_c because activated processes can still occur below this temperature. Of course, it should be remembered that all our low temperature results for the 256-atom cell correspond to nonequilibrium data, since there is a crystalline phase available.[68]

IV. LENNARD-JONES CLUSTERS

From simulations one can obtain the probability distributions of the system being in the basin of attraction of a minimum of energy E at a temperature T. As one can evaluate the partition function of a minimum within the harmonic approximation, or more accurately using anharmonic expressions,[16,70] the probability distributions can be inverted to obtain distributions for the number of minima.[16–18]

However, even if we could find a way of dividing up configuration space into basins around saddle points (i.e., without the problem of NSP's associated with the $|\nabla E|^2$ mapping), we could not find the actual distributions of the number of saddles from simulation. The missing ingredient is an expression for the partition function associated with the basin around a saddle,[71] without which probability distributions of saddles obtained from simulation cannot be inverted.

Therefore, an alternative approach is needed to obtain distributions of saddle points. Here we aim to obtain (near) complete sets of saddle points for a model finite system, namely small Lennard-Jones clusters. This task has been previously attempted for minima and transition states up to $N=13$ by Tsai and Jordan;[14] since then larger databases have been obtained for some of these clusters.[72–74] Although there are standard methods available to find minima and transition states, finding saddle points of a particular index represents a new challenge. Eigenvector-following provides an efficient way to locate transition states, where we search uphill in one direction while minimizing in the tangent space.[75] We have simply extended this approach to find a saddle point of index I by searching uphill in I orthogonal directions, while minimizing in all other directions. All the uphill directions were treated in the same way as for a transition state search, and were orthogonalized to the search direction and gradient in the tangent space minimization, requiring only minor modifications of our usual approach.[7]

To generate the sets of stationary points, we begin by obtaining samples of minima and transition states as in previous applications.[7,14,76] From these sets of stationary points we search for index two saddles after randomly perturbing the coordinates of the minima and transition states. We typically perform twenty such searches for each stationary point. We then iteratively repeat this procedure for higher-index stationary points, at each stage performing searches from all stationary points of lower index. This procedure is terminated when no stationary points of a particular index are found.

The sets of stationary points obtained in this manner are typically incomplete, and the incompleteness is larger for stationary points of lower index, for which fewer searches have been conducted. To converge the sets a reverse procedure was performed. Starting from the stationary points of highest index (I_{max}) searches are performed for saddle points of index $I_{max}-1$ following a random perturbation. Typically five searches from each stationary point are enough to ensure convergence. Searches are then performed for stationary points of index $I_{max}-2$ from all those of higher index, and so on until the searches for minima are completed. The importance of this reverse procedure is evident, for example, from the $\sim 50\%$ increase in the number of LJ_{13} transition states located when the searches from higher-index saddle points were performed.

The numbers of stationary points as a function of the saddle point index are given in Table IV. We were able to find essentially complete distributions of stationary points of any index for all clusters up to $N=9$. However, above this size the search had to be terminated at low index, because the numbers of stationary points involved are too large for a characterization of the whole distribution to be feasible. For example, extrapolation suggests that for LJ_{13} that there are of the order of 10^8 saddle points of the most common index. For these larger sizes the reverse procedure was still performed, but starting from the highest index for which we performed searches. As a result the number of saddle points of the highest index searched is likely to be much less than the true total, because no searches from saddle points of higher index have been attempted.

One particularly striking feature of the results is the large number of higher-index stationary points for systems of such small size, especially relative to the number of minima. For example, LJ_9 has ~ 800 times more index seven saddles than minima.

To quantitatively probe these distributions we plot in Fig. 2(a) the number of saddle points against the intensive measure of the saddle point index, i. For a cluster, $i=I/(3N-6)$ because there are a further three zero eigenval-

TABLE IV. Number of saddle points of each index for LJ$_N$ clusters. The numbers in italics are likely to be far from complete.

| | Stationary point index | | | | | | | | | | | | | | | |
N	0	1	2	3	4	5	6	7	8	9	10	11	12	13	14	15
4	1	1	2	1	1	0	0									
5	1	2	4	6	6	2	1	0								
6	2	3	13	24	30	26	16	5	1	0						
7	4	12	44	98	168	190	168	101	45	11	1	0				
8	8	42	179	494	1000	1458	1619	1334	852	388	125	26	1	0		
9	21	165	867	2820	6729	12 093	16 292	16 578	13 226	8286	4053	1444	376	56	1	0
10	64	635	4074	16 407	46 277	*97 183*										
11	170	2424	17 109	*47 068*												
12	515	8607	*27 957*													
13	1509	28 756	*88 079*													

ues corresponding to rotations. As is clear from Fig. 2(a) the data fits very well to the Gaussian form

$$n_{sp}(I) = n_{sp}^{max} \exp\left(-\frac{(I - I_{mid})^2}{2\sigma^2}\right). \qquad (3)$$

(a)

(b)
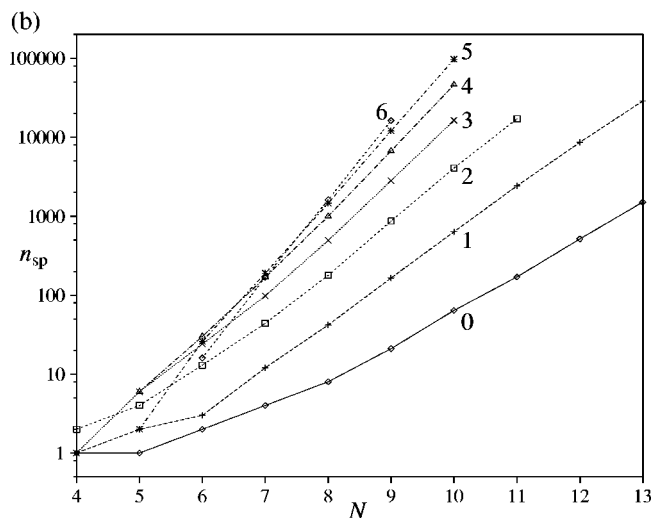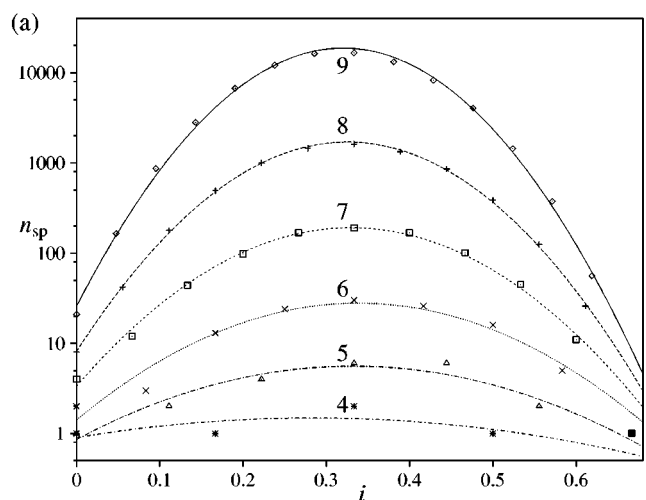
FIG. 2. The number of saddle points as a function of (a) the saddle point index and (b) the size. In (a) the data points are from Table IV, the curves are Gaussian fits to the data, each curve is labeled by the cluster size and only sizes for which we have obtained complete distributions are represented. In (b) lines are labeled by the saddle point index.

The agreement is less good for the smaller sizes, but this result is unsurprising considering the small number of stationary points.

The parameters of the Gaussian fits appear in Table V. It is particularly noteworthy that the mid-points of the distributions in Fig. 2(a) are approximately constant. $i_{mid} \approx 1/3$ which implies $I_{mid} \approx N - 2$. Of course, the tail of the Gaussian is cutoff at $I = 0$, but it is also cut off beyond $2I_{mid}$. There are no stationary points for $I > I_{max} = 2N - 4$.

Another interesting feature of the Gaussian distribution is that the standard deviation of the distributions is only a weak function of N, scaling sublinearly with size. Therefore, the distributions when considered as a function of i (rather than I), as in Fig. 2, become narrower as the size increases.

Equation (3) allows us to predict the ratio of the number of transition states to minima

$$\frac{n_{ts}}{n_{min}} = \exp\left(\frac{2I_{mid} - 1}{2\sigma^2}\right) \approx \exp\left(\frac{2N - 5}{2\sigma^2}\right). \qquad (4)$$

This ratio scales less than exponentially with N, because σ is a weakly increasing function of N. The above equation can be rearranged to obtain an expression for σ

$$\sigma \approx \sqrt{\frac{N - 5/2}{\log(n_{ts}/n_{min})}}. \qquad (5)$$

The value of σ thus obtained will, of course, involve a greater error than that obtained from fitting to the complete saddle point distribution, but it can be applied to the larger clusters for which we do not have complete distributions. Again we find that σ continues to increase slowly with N.

In Fig. 2(b) we show how the number of stationary points with a particular index depends upon N. Most of the

TABLE V. Parameters for the Gaussian fits of the distributions $n_{sp}(I)$. Results are only included for sizes that have a complete distribution.

N	n_{sp}^{max}	I_{mid}	i_{mid}	σ
4	1.49	1.700	0.283	1.699
5	5.59	2.989	0.332	1.545
6	27.9	4.063	0.339	1.663
7	191.4	4.944	0.330	1.738
8	1706	5.858	0.325	1.791
9	18782	6.728	0.320	1.853

FIG. 3. The ratio of the number of minima to transition states as a function of N.

ρ	3	4	6	10
n_{min}	7	159	1477	10 815
n_{ts}	47	1366	26 431	>218 584
n_{ts}/n_{min}	6.7	8.6	17.9	>20.2

ferent index have to be considered, and the assumption of sub-system independence becomes less plausible. Therefore we need a different approach if we are to justify the Gaussian distribution for $n_{sp}(I)$.

For any cluster there will always be a single stationary point of index $2N-4$ corresponding to a linear chain. For this configuration there are five zero Hessian eigenvalues (three translations and only two rotations), $N-1$ positive eigenvalues corresponding to bond stretches, as well as the $2N-4$ negative eigenvalues corresponding to bond-angle deformations.

The chain contains the minimum possible number of nearest-neighbor contacts for a bound configuration. To produce any more negative eigenvalues would require the dissociation of an atom, but then the system would no longer correspond to a cluster of N atoms. Therefore, the linear chain must correspond to the saddle point with the highest index, in agreement with the value of I_{max} that we found for each distribution. In fact the linear chain is rather exceptional because of its five zero eigenvalues. Any other configuration with $N-1$ bonds must be nonlinear and so has $2N-5$ negative Hessian eigenvalues, six zeros, as well as the $N-1$ positive eigenvalues. The linear chain's five zero eigenvalues allow the possibility of another negative eigenvalue.

The analysis of the linear configuration suggests that the stationary point index corresponds to the number of bond-angle degrees of freedom that have negative eigenvalues. The stationary points in Fig. 4 illustrate this trend. Of course, there are some stationary points where there are negative eigenvalues in the bond-stretch degrees of freedom, but these are in the minority.

This upper limit to I also suggests that the Gaussian distribution may be a result of the number of different ways of choosing negative eigenvalues for $2N-5$ bond-angle de-
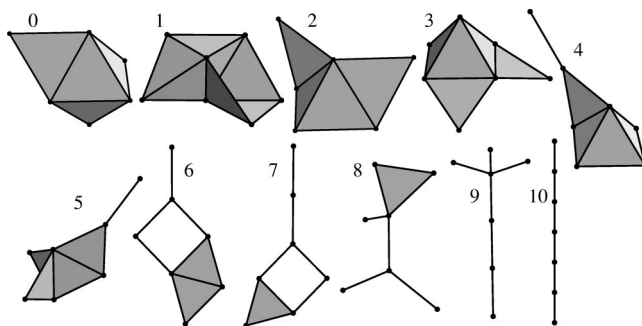
plots seem to tend to straight lines for larger N. Of course, there are likely to be significant deviations when $n_{sp}(I)$ <100, where the values could reflect peculiarities of these small sizes. Furthermore, there is insufficient data to definitely confirm an exponential scaling with size.

There is a theoretical expectation for n_{min} to scale exponentially with size.[2,15] Here we present the simple argument of Ref. 2, which applies to a sufficiently large system. If a system of mN atoms can be divided into m equivalent subsystems of N atoms, and the stable arrangements of the subsystem are effectively independent, then

$$n_{min}(mN) = n_{min}(N)^m. \tag{6}$$

The solution of this equation is

$$n_{min}(N) = \exp(\alpha N). \tag{7}$$

A similar argument can be given for the number of transition states. Assuming the rearrangements associated with the transition states can be localized to one sub-cell, the whole mN-atom system will be at a transition state when one of the subsystems is at a transition state and the rest are at a minimum. Therefore,

$$n_{ts}(mN) = m n_{min}(N)^{m-1} n_{ts}(N). \tag{8}$$

The solution of this equation is

$$n_{ts}(N) = N \exp(\alpha N). \tag{9}$$

Hence, n_{ts}/n_{min} grows linearly with size. Our databases are consistent with this trend (Fig. 3). The value of α is system dependent, and we illustrate this fact for the 13-atom cluster bound by the Morse potential, M_{13}, as a function of the range parameter, ρ. The results in Table VI supersede those in previous work,[7] and were obtained using transition state searches based on starting points obtained by considering hard sphere collisions, as described elsewhere.[21]

This approach to finding expressions for the distribution of saddles becomes more problematic for saddle points of higher index. As I increases, the equations are increasingly hard to solve, as more combinations of saddle points of dif-

FIG. 4. Some LJ_7 stationary points. Each structure is labeled by the value of I, the index of the stationary point, and each is at the midpoint of the energy distribution for stationary points of that index.
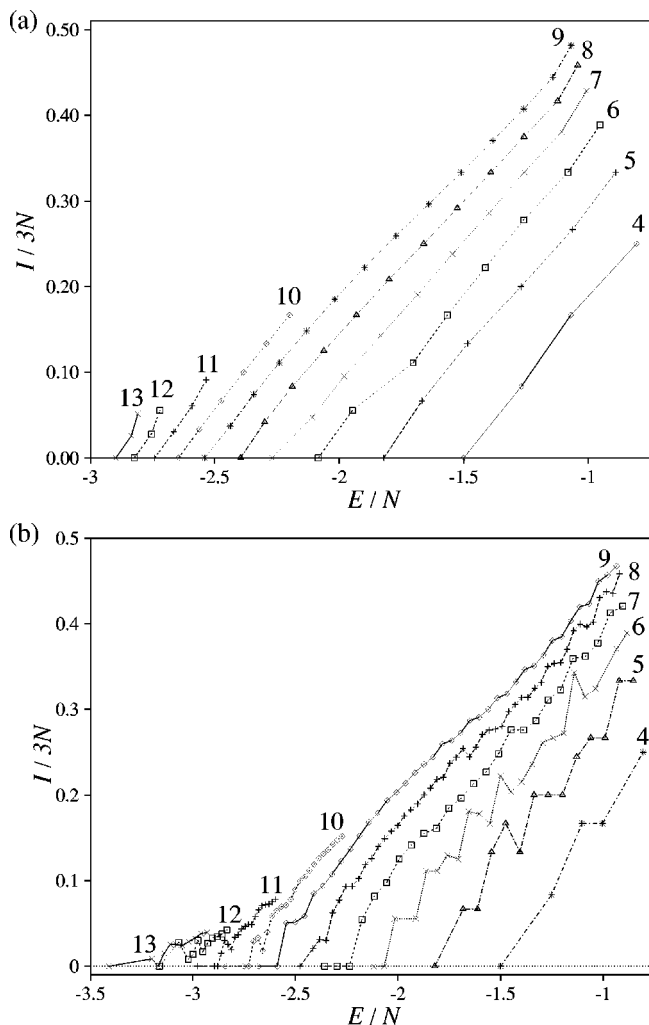
(a)

(b)

FIG. 5. $I/3N$ vs E/N. In (a) the points are averages over I and in (b) averages over the energy. In (b) the curves are cut off at $I_{max}-1/2$ for those sizes that have incomplete saddle point distributions.

grees of freedom (assuming six zero eigenvalues and $N-1$ bond stretches). This assumption gives a binomial distribution

$$n_{sp}(I) = \frac{(2N-5)!}{(2N-5-I)!I!}, \tag{10}$$

which can be well approximated by a Gaussian with

$$I_{mid} = N - 5/2,$$

$$n_{sp}^{max} = \frac{(2N-5)!}{[(N-5/2)!]^2}, \tag{11}$$

$$\sigma = \sqrt{\frac{N-5/2}{2}}.$$

This simple analysis gives properties that are in good agreement with our actual distributions. I_{mid} almost exactly matches the observed value and σ is a weakly increasing function of N. The main error is the result that $n_{sp}(0) = n_{sp}(2N-5) = 1$. This error occurs because even when we have the maximum or minimum number of bond-angle degrees of freedom with negative eigenvalues, there are still a
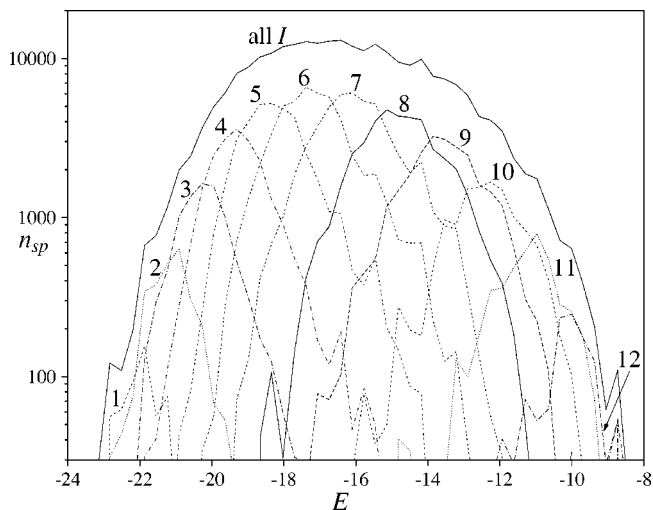

FIG. 6. The number of LJ$_9$ saddle points of index I as a function of energy. Each curve is labeled by the index I, except for the sum of all the distributions.

number of different structural ways that this can be achieved [roughly $\exp(\alpha N)$ in fact]. Therefore, to correct for this error, the above expression for n_{sp}^{max} can be multiplied by an exponential function fitted to the number of minima. Also, the Gaussian fit to the binomial distribution gives the erroneous prediction that n_{ts}/n_{min} is independent of N. However, the binomial distribution itself gives the correct result, while the Gaussian approximation begins to break down at the tails of the distribution.

One quantity that has been focused upon in previous studies of saddle points in glasses has been the variation of the saddle point index with potential energy.[33,34,41] The averaging performed to obtain this function can be done in two ways. One can either look at $\langle E(I) \rangle$, the average energy of saddles with index I [Fig. 5(a)], or at $\langle I(E) \rangle$, the average index of stationary points with energy E [Fig. 5(b)]. For $N \geq 10$ as the energy increases the latter function saturates at the highest index for which we have performed searches. To avoid this effect of the incomplete distributions, we have cut off the function at $I_{max}-1/2$.

Both averages show an approximately linear increase of the energy with saddle point index, similar to that observed for supercooled liquids.[33,34,41] However, the slope is somewhat lower for $\langle I(E) \rangle$, because the energy at which saddle points of a particular index are the most common does not necessarily correspond to the energy at the maximum of their distribution i.e., $\langle E(I) \rangle$ (Fig. 6). For $I < I_{mid}$ the majority of the range for which they are most numerous has $E < \langle E(I) \rangle$ and for $I > I_{mid}$ has $E > \langle E(I) \rangle$.

The slopes of curves such as those in Fig. 5 have been interpreted in terms of a characteristic barrier height for the PES.[34,40,41] As the lines in Fig. 5 have similar slopes this "barrier" is only a weak function of cluster size. However, there is of course a distribution of barrier heights.[21,22] Furthermore, the experimentally observed activation energy to structural relaxation is unlikely to correspond to a barrier associated with a single rearrangement, but to the overall barrier associated with a sequence of rearrangements.[7,77]

It is also easy to show that the average barrier between minima and transition states, $\langle \Delta \rangle$, is different from the slope of Fig. 5(a):

$$\langle \Delta \rangle = \langle E_{ts} \rangle - \sum_i n_{ts}^i E_{min}^i / 2 n_{ts}, \tag{12}$$

$$\neq \langle E_{ts} \rangle - \langle E_{min} \rangle, \tag{13}$$

where E_{min}^i is the energy of minimum i and n_{ts}^i is the number of transition states connected to that minimum. $\langle \Delta \rangle$ is likely to be larger because the average over minima in the second term of Eq. (12) is usually weighted towards the lower-energy minima, since they are connected to more transition states. For example, for LJ$_{13}$ $\langle \Delta \rangle = 1.771\epsilon$, whereas $\langle E_{ts} \rangle - \langle E_{min} \rangle = 0.728\epsilon$.

Another property of saddle points that has received attention is the lowest eigenvalue of the Hessian. For a binary Lennard-Jones liquid a linear decrease in the average value of the lowest Hessian eigenvalue was observed as the energy is increased above the threshold energy at which higher-index saddle points were first observed.[34] This result is equivalent to a linear decrease with i. The behavior of this property for our cluster saddle points is depicted in Fig. 7. The curves seem to have a common form, in which the lowest eigenvalue reaches a minimum close to I_{mid}. However, these values of i are much larger than those probed in Ref. 34, and the initial parts of the curves in Fig. 7 seem to show greater linearity as the size is increased.

V. DISCUSSION

So far we have examined the properties of a particular mapping that attempts to provide a definition of the neighborhood of a saddle point, and looked at the properties of higher-index saddle points for systems where we can obtain essentially complete distributions. Here, we want to think more about the role of higher-index saddle points in the dynamics, assuming that one could find a mapping that divides all of the PES in neighborhoods around the closest saddle.
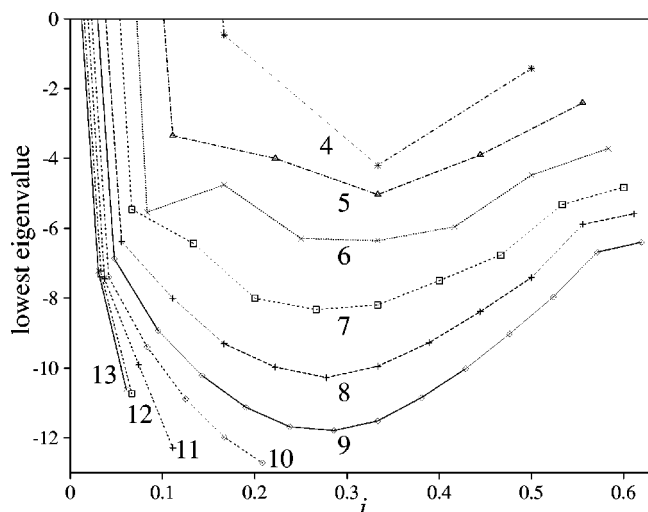

FIG. 7. The average of the lowest eigenvalue of the Hessian for saddle points of the same index as a function of i. The different curves correspond to different sizes as labeled. The eigenvalues are in units of ϵ/σ^2.

First we review the relevant aspects of the inherent structure approach to the dynamics, i.e., in terms of the dynamics of transitions between the basins of attraction surrounding minima. This approach can be formulated in terms of a master equation[78] describing the evolution of the occupation probability of a particular minimum in terms of the rates of probability flow into and out of that minimum[7,79]

$$\frac{dP_i(t)}{dt} = \sum_{j \neq i} [k_{ij} P_j(t) - k_{ji} P_i(t)], \tag{14}$$

where P_i is the occupation probability of the basin around minimum i and k_{ij} is the rate constant for a transition from basin j to basin i. This set of equations can then be solved to give a complete picture of the inter-minimum dynamics.

The only assumption that this approach relies upon is the Markovian nature of the underlying dynamics, i.e., the probability of the transition $i \to j$ must not depend on the history of reaching minimum i, so that the k_{ij} are constants for a given temperature or energy. This assumption will certainly be true when states within a basin of attraction equilibrate on a time scale faster than transitions to different minima, i.e., $\tau_{inter} \gg \tau_{intra}$, where these two time scales are for interbasin and intrabasin relaxation. Indeed, it is this separation of time scales that makes the inherent structure approach a natural way to describe the dynamics. The breakdown of the Markovian character of the interbasin dynamics places an upper bound on the temperature for which this approach is applicable. Previous results for small alkali halide and LJ clusters show reasonable agreement between MD rates and model rate theory for relatively high energies.[80,81]

In the above theory for isomerization rates there is no requirement for the system to lie close to the minimum in configuration space. During the occupancy of a given catchment basin the system could be found, on average, close to the boundary. Therefore, the increase in I with temperature seen for supercooled liquids above a threshold temperature does not necessarily imply that the inherent structure dynamics approach has broken down. Rather the test is whether the interbasin dynamics are no longer Markovian.

One of the main advantages of Eq. (14) is that we can draw on the mature field of unimolecular rate theory[82] to calculate the k_{ij}. For example, the classical limits for the microcanonical and canonical Rice–Ramsperger–Kassel–Marcus rate constants in the harmonic approximation are[82]

$$k(E) = \left(\frac{E - E^\dagger}{E} \right)^{s-1} \frac{\bar{\nu}^s}{\bar{\nu}_\dagger^{s-1}},$$

$$k(T) = \exp(-E^\dagger/kT) \frac{\bar{\nu}^s}{\bar{\nu}_\dagger^{s-1}}, \tag{15}$$

where E and $E^\dagger$ are the total energy and the potential energy of the transition state relative to the energy of the minimum, s is the number of vibrational degrees of freedom, and $\bar{\nu}$ and $\bar{\nu}_\dagger$ are the geometric mean vibrational frequencies of the minimum and transition state, respectively.

Angelani et al. have argued that "diffusion is entropy driven, even below T_{MCT}" based on the observation that the instantaneous potential energy of the system lies well above the SP's obtained by minimizing $|\nabla E|^2$.[33] However, increas-

ingly large values of the total energy are needed to obtain significant rates as the number of degrees of freedom increases (see, for example[83]), as is clear from Eqs. (15). To maintain a finite microcanonical rate constant as s rises the ratio $E/E^\dagger$ must increase. From the canonical viewpoint, the higher total energy is simply required to maintain a constant temperature as the system size grows.

In the microcanonical ensemble the entropy is the appropriate thermodynamic potential, while in the canonical ensemble we must instead consider free energy barriers, although it should be remembered that the two ensembles are equivalent in the bulk limit. The relative energies of the transition state and minimum, and the widths of the minimum and transition state valley contained in the ratio of frequencies, contribute to the rate constant for an elementary unimolecular isomerization in both ensembles. Both are included in the standard rate expressions above. However, the relative importance of different contributions to $k(E)$ cannot be assessed without considering how the different terms scale with system size. For the canonical rate constant $k(T)$, where it is meaningful to consider separate entropic and energetic contributions to the free energy barrier, the total energy does not enter. The energy difference, $E^\dagger$, for a particular class of rearrangement should be an intensive rather than an extensive quantity.

For normal liquids above the melting point Dzugutov has demonstrated a strong empirical correlation between the entropy and the diffusion constant.[84] Other recent simulation studies[10,19,53] have been interpreted using the Adam–Gibbs model,[85] where the entropy, or part of it, enters in a rather different way through heuristic arguments. On the other hand, atomic diffusion in solids is routinely treated by Vineyard's approach,[86] which is simply an application of conventional unimolecular rate theory to bulk. There is clearly a pressing need to determine the limit of applicability of standard rate theory to supercooled liquids, and to develop alternative approaches with a firm microscopic basis where necessary.

Cavagna has suggested that when $\tau_{\text{inter}} \sim \tau_{\text{intra}}$ it is more appropriate to think about the dynamics in terms of transitions between the neighborhoods of saddle points.[29] As Eq. (14) can be applied to any partition of the PES into "basins," not just those surrounding minima, a similar formalism can be developed as long as the inter-saddle dynamics are Markovian. However, therein lies the problem. If the residence times in the basins of attraction surrounding a minimum are too short for equilibrium between the vibrational modes to be established, it seems even less likely that the necessary separation of time scales will hold for basins surrounding saddle points. By definition, there are forces acting to take the system out of such regions. Furthermore, in contrast to the case of isomerizations between minima, there is no established theory for transition rates between saddles. In fact, it is unclear how to calculate the partition function for the catchment basin of a saddle, which would surely be necessary to evaluate rate constants. It is, therefore, hard to see how this view of the dynamics can be put on a quantitative footing. In his contribution Cavagna simply speculated that the inter-saddle rate constants would increase as I increased.[29]

One other possible criticism of the "saddles-ruled" approach of Cavagna is that it seems to ignore many of the effects of the topography of the PES, and so seems to conflict with much of the recent work that has emphasized the importance of this topography.[5,9,10] For example, Cavagna suggests that the origin of strong and fragile behavior[87] simply lies in the value of the thermal energy at the temperature for which saddles begin to be frequently sampled relative to the "barrier" obtained from the slope of the line giving the averaged dependence of the index upon the saddle point energy.[29]

It is also too simplistic to suggest that the index of a saddle indicates the "number of diffusive directions." [33] In fact, rearrangements may be both diffusive and nondiffusive in nature,[21] and the character can only be diagnosed by calculating steepest-descent paths connecting the relevant stationary points, not from purely local information. The nondiffusive transitions typically involve an atom moving slightly within the cage of its neighbors.

VI. CONCLUSIONS

We have examined in detail the behavior of the $|\nabla E|^2$ mapping of configurations to saddle points, and find that it has a number of shortcomings. We agree with Cavagna[29] that the mapping cannot partition the whole of the PES into basins surrounding the saddle points, as claimed by Angelani et al.[33] In fact, for the systems we have studied the vast majority of configuration space sampled by the supercooled liquid is mapped on to points that are not stationary points of the PES. Furthermore, the saddle points obtained by this mapping are no closer to the initial configuration than are the the transition states and minima that we located. Therefore, the mapping does not seem to satisfy the requirement of dividing the PES into neighborhoods around the closest saddle. We have also pointed out problems with a number of interpretations suggested in previous work.

A more straightforward way to characterize the properties of higher-index saddles is for systems where complete distributions of saddle points can be obtained. Our results for LJ clusters reveal that the distributions are a Gaussian function of the index, as well as of the energy.[17,18] Gaussian index distributions have also been found for random matrices.[88] We have suggested an explanation for this distribution in terms of the number of possible ways of assigning negative eigenvalues to a set of bond-angle degrees of freedom. We find an approximately linear relationship between the potential energy of the saddle point and its index, similar to the results for supercooled liquids.

We do not think that a description of the dynamics in terms of inter-saddle, rather than inter-minimum, transitions will offer any advantages, even if a proper partitioning of the PES into catchment basins of saddles can be devised. Although the temperature at which the dynamics become non-Markovian, and hence the linear master equation formalism breaks down, has not yet been established it may well be at temperatures where the time scale for transitions between minima is comparable to the time for equilibrium to be established between the vibrational modes. Below this regime we should be able to apply standard unimolecular rate theory,

but above it any approach focusing on uncorrelated transitions between local regions of configuration space is likely to fail. Other approaches, such as mode-coupling theory,[35–37] will then be more appropriate.

ACKNOWLEDGMENTS

[1] M. Goldstein, J. Chem. Phys. **51**, 3728 (1969).
[2] F. H. Stillinger and T. A. Weber, Phys. Rev. A **25**, 978 (1982).
[3] F. H. Stillinger and T. A. Weber, Science **225**, 983 (1984).
[4] J. N. Murrell and K. J. Laidler, Trans. Faraday Soc. **64**, 371 (1968).
[5] P. G. Debenedetti and F. H. Stillinger, Nature (London) **410**, 259 (2001).
[6] F. H. Stillinger, Science **267**, 1935 (1995).
[7] D. J. Wales et al., Adv. Chem. Phys. **115**, 1 (2000).
[8] C. L. Brooks III, J. N. Onuchic, and D. J. Wales, Science **293**, 612 (2001).
[9] S. Sastry, P. G. Debenedetti, and F. H. Stillinger, Nature (London) **393**, 554 (1998).
[10] S. Sastry, Nature (London) **409**, 164 (2001).
[11] W. Kob, F. Sciortino, and P. Tartaglia, Europhys. Lett. **49**, 590 (2000).
[12] F. Sciortino and P. Tartaglia, Phys. Rev. Lett. **86**, 107 (2001).
[13] M. R. Hoare and J. McInnes, Adv. Phys. **32**, 791 (1983).
[14] C. J. Tsai and K. D. Jordan, J. Phys. Chem. **97**, 11227 (1993).
[15] F. H. Stillinger, Phys. Rev. E **59**, 48 (1999).
[16] J. P. K. Doye and D. J. Wales, J. Chem. Phys. **102**, 9659 (1995).
[17] F. Sciortino, W. Kob, and P. Tartaglia, Phys. Rev. Lett. **83**, 3214 (1999).
[18] S. Büchner and A. Heuer, Phys. Rev. E **60**, 6507 (1999).
[19] A. Scala et al., Nature (London) **406**, 166 (2000).
[20] I. Saika-Voivod, P. H. Poole, and F. Sciortino, Nature (London) **412**, 514 (2001).
[21] T. F. Middleton and D. J. Wales, Phys. Rev. B **64**, 024205 (2001).
[22] N. Mousseau (cond-mat/0004356).
[23] T. Keyes, J. Phys. Chem. A **101**, 2921 (1997).
[24] J. D. Gezelter, E. Rabani, and B. J. Berne, J. Chem. Phys. **107**, 4618 (1997).
[25] T. Keyes, W.-X. Li, and U. Zurcher, J. Chem. Phys. **109**, 4693 (1998).
[26] J. D. Gezelter, E. Rabani, and B. J. Berne, J. Chem. Phys. **109**, 4695 (1998).
[27] C. Donati, F. Sciortino, and P. Tartaglia, Phys. Rev. Lett. **85**, 1464 (2000).
[28] E. La Nave et al., Phys. Rev. E **64**, 036102 (2001).
[29] A. Cavagna, Europhys. Lett. **53**, 490 (2001).
[30] J. Kurchan and L. Laloux, J. Phys. A **29**, 1929 (1996).
[31] T. A. Weber and F. H. Stillinger, Phys. Rev. B **31**, 1954 (1985).
[32] J. W. McIver and A. Komornicki, J. Am. Chem. Soc. **94**, 2625 (1972).
[33] L. Angelani et al., Phys. Rev. Lett. **85**, 5356 (2000).
[34] K. Broderix et al., Phys. Rev. Lett. **85**, 5360 (2000).
[35] W. Götze, in Liquids, Freezing and the Glass Transition, Les Houches, Session LI, 1989, edited by J.-P. Hansen, D. Levesque, and J. Zinn-Justin (North-Holland, Amsterdam, 1991), pp. 287–499.
[36] W. Kob, ACS Symp. Ser. **676**, 28 (1997).
[37] W. Götze, J. Phys.: Condens. Matter **11**, A1 (1999).
[38] A. Scala et al. (cond-mat/0106065).
[39] R. Di Leonardo et al. (cond-mat/0106214).
[40] L. Angelani, R. Di Leonardo, G. Parisi, and G. Ruocco, Phys. Rev. Lett. **87**, 055502 (2001).
[41] T. S. Grigera, A. Cavagna, I. Giardina, and G. Parisi (cond-mat/0107198).
[42] P. Shah and C. Chakravarty, J. Chem. Phys. **115**, 8784 (2001).
[43] K. Müller and L. D. Brown, Theor. Chim. Acta **53**, 75 (1979).
[44] J.-Q. Sun, K. Ruedenberg, and G. J. Atchity, J. Chem. Phys. **99**, 5276 (1993).
[45] D. J. Wales, J. Chem. Phys. **101**, 3750 (1994).

[46] K. Ruedenberg and J.-Q. Sun, J. Chem. Phys. **100**, 5836 (1994).
[47] J.-Q. Sun and K. Ruedenberg, J. Chem. Phys. **98**, 9707 (1993).
[48] D. Passerone and M. Parrinello, Phys. Rev. Lett. **87**, 108302 (2001).
[49] The stationary points of the Müller–Brown surface reported in Ref. 45 are correct but their energies are not. This bug does not affect any conclusions of Ref. 45.
[50] F. S. Acton, Numerical Methods that Work (Mathematical Association of America, Washington, 1990).
[51] T. B. Schrøder, S. Sastry, J. C. Dyre, and S. C. Glotzer, J. Chem. Phys. **112**, 9834 (2000).
[52] W. Kob and H. Andersen, Phys. Rev. Lett. **73**, 1376 (1994).
[53] S. Sastry, Phys. Rev. Lett. **85**, 590 (2000).
[54] S. Sastry, J. Phys.: Condens. Matter **12**, 6515 (2000).
[55] H. Jonsson and H. C. Andersen, Phys. Rev. Lett. **60**, 2295 (1988).
[56] W. Kob and H. C. Andersen, Phys. Rev. E **51**, 4626 (1995).
[57] W. Kob and H. Andersen, Phys. Rev. E **52**, 4134 (1995).
[58] C. Donati et al., Phys. Rev. E **60**, 3107 (1999).
[59] C. A. Angell, B. E. Richards, and V. Velikov, J. Phys.: Condens. Matter **11**, A75 (1999).
[60] F. Sciortino, W. Kob, and P. Tartaglia, J. Phys.: Condens. Matter **12**, 6525 (2000).
[61] S. Büchner and A. Heuer, Phys. Rev. Lett. **84**, 2168 (2000).
[62] S. D. Stoddard and J. Ford, Phys. Rev. A **8**, 1504 (1973).
[63] D. Liu and J. Nocedal, Math. Program. B **45**, 503 (1989).
[64] L. J. Munro and D. J. Wales, Phys. Rev. B **59**, 3969 (1999).
[65] Y. Kumeda, D. J. Wales, and L. J. Munro, Chem. Phys. Lett. **341**, 185 (2001).
[66] A. Cavagna, I. Giardina, and G. Parisi, J. Phys. A **34**, 5317 (2001).
[67] W. H. Press, B. P. Flannery, S. A. Teukolsky, and W. T. Vetterling, Numerical Recipes (Cambridge University Press, Cambridge, 1986).
[68] T. F. Middleton, J. Hernández-Rojas, P. N. Mortenson, and D. J. Wales, Phys. Rev. B **64**, 184201 (2001).
[69] A. Cavagna, I. Giardina, and G. Parisi, Phys. Rev. B **57**, 11251 (1998).
[70] F. Calvo, J. P. K. Doye, and D. J. Wales, J. Chem. Phys. **115**, 9627 (2001).
[71] The contribution to the partition function for a basin surrounding a saddle point from the space orthogonal to the unstable modes is easy to evaluate, and the expression is the same as for a minimum with the dimension of this reduced space. However, the contribution from the space spanned by the unstable modes is unclear. One approximation that has been used for transition states is to assume a flat valley of a certain length in the direction of the transition vector (Refs. 16 and 89), and this approach could be extended to all unstable modes.
[72] D. J. Wales and J. P. K. Doye, J. Chem. Phys. **106**, 5296 (1997).
[73] K. D. Ball and R. S. Berry, J. Chem. Phys. **111**, 2060 (1999).
[74] S. F. Chekmarev, Phys. Rev. E **64**, 036703 (2001).
[75] C. J. Cerjan and W. H. Miller, J. Chem. Phys. **75**, 2800 (1981).
[76] M. A. Miller, J. P. K. Doye, and D. J. Wales, J. Chem. Phys. **110**, 328 (1999).
[77] M. A. Miller, J. P. K. Doye, and D. J. Wales, Phys. Rev. E **60**, 3701 (1999).
[78] N. G. V. Kampen, Stochastic Processes in Physics and Chemistry (North Holland, Amsterdam, 1992).
[79] R. S. Berry and R. E. Breitengraser-Kunz, Phys. Rev. Lett. **74**, 3951 (1995).
[80] J. P. Rose and R. S. Berry, J. Chem. Phys. **96**, 517 (1992).
[81] M. A. Miller and D. J. Wales, J. Chem. Phys. **107**, 8568 (1997).
[82] T. Baer and W. L. Hase, Unimolecular Reaction Dynamics (Oxford University Press, Oxford, 1996).
[83] A. Baba et al., J. Chem. Phys. **106**, 3329 (1997).
[84] M. Dzugutov, Nature (London) **381**, 137 (1996).
[85] G. Adam and J. H. Gibbs, J. Chem. Phys. **43**, 139 (1965).
[86] G. H. Vineyard, J. Phys. Chem. Solids **3**, 121 (1957).
[87] C. A. Angell, J. Non-Cryst. Solids **131–133**, 13 (1991).
[88] A. Cavagna, J. P. Garrahan, and I. Giardina, Phys. Rev. B **61**, 3960 (2000).
[89] S. F. Chekmarev and I. H. Umirzakov, Z. Phys. D: At., Mol. Clusters **26**, 373 (1993).